Shear properties of the re-entrant auxetic structure made via electron beam melting

[1]Li Yang, [2]Ola Harrysson, [2]Harvey West, [3]Denis Cormier
[1]University of Louisville, Louisville, KY 40292
[2]North Carolina State University, Raleigh, NC 27695
[3]Rochester Institute of Technology, Rochester, NY, 14623

Abstract

While the tensile/compressive mechanical properties of the re-entrant auxetic cellular structure have been relatively well modeled, their shear properties including the shear modulus and shear strength have not been investigated. This paper focuses on the analytical modeling of the shear properties of this auxetic structure utilizing beam analysis. The modeling results were further compared with results from both simulation and experimentation. It was found that in addition to the effective length reduction effect, the size effect also becomes significant for the shearing of this re-entrant auxetic structures. Due to the size effect, it was expected that the re-entrant auxetic structure could not be effectively homogenized based on the developed analytical property model, and additional design factors must be considered in the future.

Introduction

In industries such as aerospace and automotive, cellular structures are widely used due to their outstanding compromise between mechanical properties and weight. Often, the cellular structures are used as cores in sandwich panel structures in order to achieve satisfactory combination of various requirements including bending stiffness, energy absorption, ultimate strength and weight. Various literature works have been dedicated to the characterization of cellular cores and their applications in sandwich structures [1-8]. Of specific interest are the pre-modeled periodic cellular structures, which can be designed and optimized according to specific requirements. Unlike random cellular structures whose properties are often controlled via empirical production quality control, periodic cellular structures possess definitive geometrical patterns, making it possible to perform property analysis with the structures during the design stage. Because of their geometrical patterns, periodic cellular structures can often be represented by unit cells. This provides a convenient alternative to analyze and optimize these cellular structures when size effect is also taken into account [9-13].

Regular honeycomb structure has been studied extensively by various researchers, and their mechanical properties are well known [2-3, 14-16]. These research works on the honeycomb

structure are mainly focused on 2D honeycomb extruded structure, in correspondence to the primary industrial manufacturing processes. Recently, other structures have been drawing increased attentions due to their potential to provide equivalent or superior properties compared to honeycomb structures [17-27]. One of such examples are auxetic structures, which are structures that exhibit negative Poisson's ratios [28]. Auxetic structures are expected to exhibit many attractive properties, such as high shear modulus [28-30], high indentation resistivity [31-32], high fracture toughness [33] and high energy absorption [34-37]. Of special interest are their exceptional shear properties since the flexure performance of the sandwich panels are largely determined by their shear strength. For lightweight sandwich structures, core shear is often the dominating failure mechanism [1], therefore a core structure with high shear strength is highly desired.

There has been some attempts to use auxetic cellular structure as core for sandwich panels in aircraft wings, in an effort to realize compliant wing design with adequate strength [38-42]. Despite the fact that rather arbitrary design parameters of the auxetic cellular structures were used in these works, the finite element analysis results suggested promising results for the design of compliant "morphing" wing structures. From these works it becomes apparent that the lack of methods to describe the shear properties of the auxetic structure has become a restriction for many application oriented works towards broader adoption of this type of structures. To date there has been relatively few works that focuses on the modeling of shear properties for auxetic structures. Scarpa et al. performed a series of experimental work with the shear properties of various auxetic structures, and employed both empirical and FEA model to describe the shear properties of the structures [43, 44]. In another work performed by the same group, the shear modulus in a specific direction of an orthotropic auxetic structure was modeled analytically using Voigt-Reuss bounds method [45]. The analysis yield a rather wide range of modulus values, which could potentially restrict the accuracy of the design prediction of this type of structure. Xu et al. applied homogenization method on a 2D extruded re-entrant auxetic cellular structure. By ignoring the effect of the face sheet, the shear moduli of the auxetic cellular structure on both non-extrusion directions were derived, although no experiment or numerical analysis were performed for verification [46].

In this work, attempt was made to model the shear properties of a 3D re-entrant auxetic structure. Analytical predictions were compared with the FEA analysis results as well as experiments in order to verify the modeling accuracy. This will enable the design of sandwich panel structure for specific shear performance using the auxetic cellular structure. Previous modeling work on this structure has established the design equations that determine the elastic modulus and compressive strength of the structure, which was verified by experiments and FEA analysis with satisfactory results [47-49]. Therefore, the results from this work could also potentially enable the homogenization of the structure, which will be briefly discussed in this paper as well.

Shear properties modeling

The unit cell of the re-entrant auxetic structure is shown in Fig.1a, and the geometrical design parameters are shown in Fig.1b, which include the lengths of the vertical and re-entrant struts H and L, respectively, the re-entrant angle θ between the two types of strut, and the cross sectional shape and dimensions of the struts (not shown). Same design approach as previously employed was adopted to model the shear performance of the structure [47-49]. However, as the standard unit cell as shown in Fig.1a lacks sufficient symmetry under the shearing conditions, a modified unit cell geometry with offset boundaries as shown in Fig.1c was used in order to simplify the modeling analysis. For a spatially infinite cellular structure, under remote shear stresses τ, it can be easily shown that the modified unit cell structure is subject to force components as shown in Fig.2a. The re-entrant struts aligning at different directions in relation to the shear stress also exhibit different loading conditions, which are marked as type A and B in Fig.2a. While type A struts align at an angle in relation to the shear plane, type B struts align along the shear plane. As type A struts are not subject to effective loading, it does not contribute to the deformation and strength of the structures under this loading condition.

Fig.2b and Fig.2c show the loading of a half vertical strut and a half re-entrant strut, respectively. From force equilibrium these force components can be readily determined as:

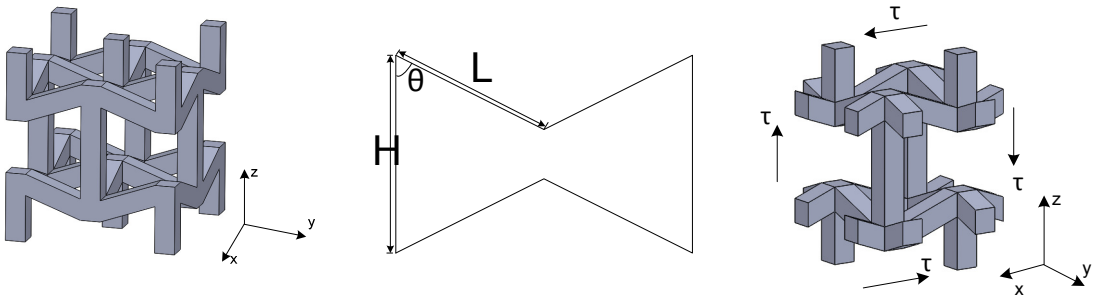

(a) The unit cell (b) Parameter of a unit cell (c) Shear of structure

Fig.1 3D re-entrant auxetic unit cell design

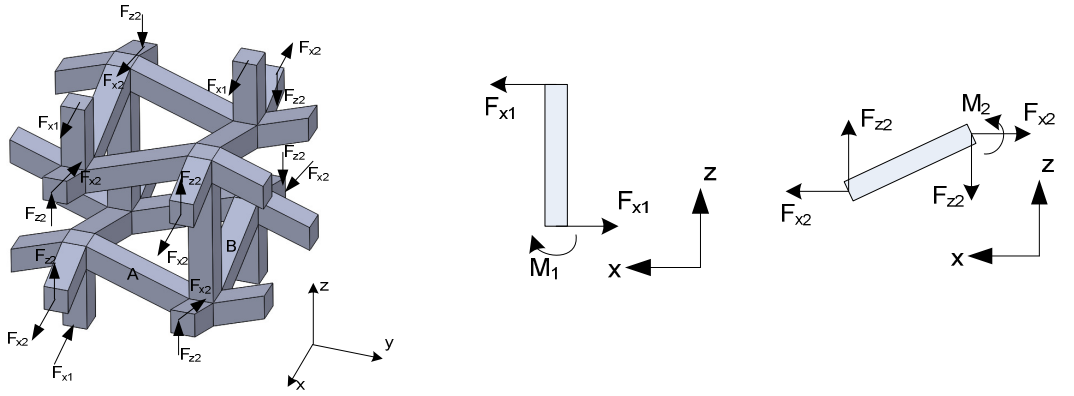

(a) Vertical strut (b) Vertical strut (half) (c) Type B re-entrant strut (half)

Fig.2 Decomposition of unit cell struts and force components

$$F_{x1} = 2\tau L^2 \sin^2\theta \qquad (1)$$

$$F_{x2} = \frac{1}{2}F_{x1} = \tau L^2 \sin^2\theta \qquad (2)$$

$$F_{z2} = \tau L \sin\theta (H - L\cos\theta) \qquad (3)$$

$$M_1 = \tau H L^2 \sin^2\theta \qquad (4)$$

$$M_2 = \frac{1}{2}\tau L^3 \sin^2\theta\cos\theta + \frac{1}{2}\tau L^2 \sin^2\theta(H - L\cos\theta) = \frac{1}{2}\tau H L^2 \sin^2\theta \qquad (5)$$

From Eq.(1)-(5), the deflection of the half struts in the x and z directions can be determined by considering both shear and bending induced deformations. Referring to Fig.3, the deflections Δx_1, Δx_2, Δz_1 and Δz_2 are:

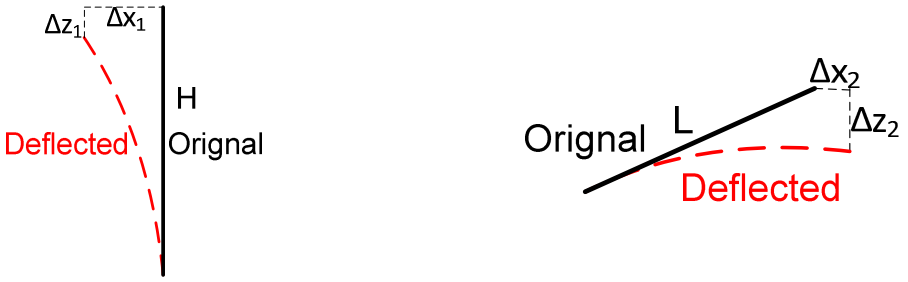

(a) Vertical strut (b) Re-entrant strut

Fig.3 Deflection of struts

$$\Delta x_1 = \frac{H}{4}\left(\frac{M_1 H}{12E_s I_v} + \frac{6F_{x1}}{5G_s A_v}\right)^2 \qquad (6)$$

$$\Delta z_1 = \frac{H}{2}\left(\frac{M_1 H}{12E_s I_v} + \frac{6F_{x1}}{5G_s A_v}\right) \qquad (7)$$

$$\Delta x_2 = \frac{L}{2}\sin\theta\left(\frac{M_2 L}{12E_s I_r} + \frac{6(F_{x2}\cos\theta + F_{z2}\sin\theta)}{5G_s A_r}\right) \qquad (8)$$

$$\Delta z_2 = \frac{L}{2}\cos\theta\left(\frac{M_2 L}{12E_s I_r} + \frac{6(F_{x2}\cos\theta + F_{z2}\sin\theta)}{5G_s A_r}\right) \qquad (9)$$

where E_s, G_s are the elastic modulus and shear modulus of the solid material, I_v, I_r are the second moment of inertia of the vertical and re-entrant struts, and A_v and A_r are the cross sectional

areas of the vertical and re-entrant struts, respectively. Note that the deflection values shown in Fig.(6)-(9) only represent these from half struts.

As the total deflection of the unit cell in each direction is contributed by two re-entrant struts and two vertical struts. Therefore, from Eq.(6)-(9) the total deflections of the unit cell structures can be determined, which can be used subsequently for the prediction of modulus.

Xz-Shear Modulus

When the deflection angle is small as is the case for some metals, Δz_1 can be neglected. Therefore, the shear modulus of the structure could be determined as:

$$G_{xz} = \frac{\tau}{\gamma} = \frac{\tau}{\frac{4\Delta x_2}{2(H - L\cos\theta)} + \frac{4\Delta z_1}{2L\sin\theta}} = \frac{\tau}{\frac{2\Delta x_2}{(H - L\cos\theta)} + \frac{2\Delta z_1}{L\sin\theta}} \tag{10}$$

Note that in Eq.(10) the deflection Δz2 does not contribute to the total deflection as this deflection is cancelled out during the deflection of the entire structure. Fig.4 shows the relationship between H/L ratio, re-entrant angle θ and the normalized shear modulus of the re-entrant auxetic structure under xz-shear. It is obvious that larger re-entrant angle and smaller H/L ratio contribute to larger shear modulus.

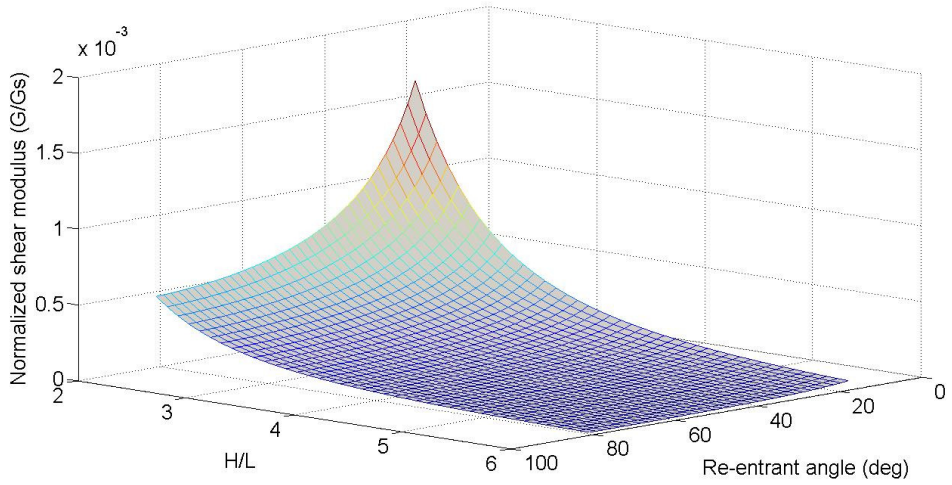

Fig.4 xz-shear modulus under different geometrical designs
L=5mm, square strut cross section, t=1mm

Xz-Shear strength

From the force analysis, the structure could be potentially subject to plastic failure (yield) and elastic failure (buckling). However, further analysis shows that the struts that are subject to compressive stress (i.e. type B re-entrant strut) are also subject to bending and shearing simultaneously, which would cause bending of the struts. Therefore, the only failure mode for

the re-entrant auxetic structures under xz-shear is plastic failure. Consequently, the shear strength of the structure can be considered as the maximum stress at which either the vertical struts or the re-entrant struts yields.

Under the loading shown in Fig.2b, vertical struts are subject to both normal stress and shear stress, which are attributed by the bending moments and the shear forces. For the simplicity of discussion, the cross section of the cellular struts was assumed to be square with thickness of t. The normal stress distribution as a function of the thickness of the strut could be determined as:

$$\sigma_v = \frac{M_1 T}{I_v} \text{ (0<T<t/2)} \tag{11}$$

where σ_v is the normal stress, and T is the thickness of the position of interest. On the other hand, the shear stress distribution as a function of the thickness of the strut could be obtained as:

$$\tau_v = \frac{3F_{x1}}{2A_v}\left(1-\frac{4T^2}{t^2}\right) \text{ (0<T<t/2)} \tag{12}$$

Define the failure of the vertical struts to occur when the first principal stress equals the yield stress of the material, or $\sigma_1=\sigma_{YS}$. The principal stress as a function of the cross sectional position T could be determined by Eq.(13) as:

$$\begin{aligned}\sigma_1 &= \frac{M_1 T}{2I_v}+\frac{1}{2}\sqrt{\frac{M_1^2T^2}{I_v^2}+\frac{9F_{x1}^2}{A_v^2}\left(1-\frac{4T^2}{t^2}\right)^2} \\ &= \frac{3\tau L^2\sin^2\theta}{t^2}\left(\frac{2HT}{t^2}+\sqrt{\frac{4H^2T^2}{t^4}+\left(1-\frac{4T^2}{t^2}\right)^2}\right)\end{aligned} \text{ (0<T<t/2)} \tag{13}$$

Therefore, maximum shear stress can be determined as:

$$\tau_m = \frac{t^2}{3\tau L^2\sin^2\theta\left(\frac{2HT}{t^2}+\sqrt{\frac{4H^2T^2}{t^4}+\left(1-\frac{4T^2}{t^2}\right)^2}\right)}\sigma_{YS} \text{ (0<T<t/2)} \tag{14}$$

For different design, the critical position will differ, and could be fully determined by Eq.(14). When H is large compared to t, the principal stress will be dominated by normal stress, therefore, the critical stress will occur at the surface of the vertical strut (T=t/2), which can be determined as:

$$\tau_m = \frac{t^3}{6\tau HL^2\sin^2\theta}\sigma_{YS} \tag{15}$$

For type B re-entrant struts, from the loading shown in Fig.2c, the normal stress and shear stress can be determined in similar manner as:

$$\sigma_r = \pm\frac{M_2 T}{I_r} + \frac{F_{x2}\sin\theta - F_{z2}\cos\theta}{A_r} \quad (0<T<t/2) \tag{16}$$

$$\tau_r = \frac{3(F_{x2}\cos\theta + F_{z2}\sin\theta)}{2A_r}\left(1-\frac{4T^2}{t^2}\right) \quad (0<T<t/2) \tag{17}$$

Note that in Eq.(16) positive and negative signs of the stress status represent tensile and compressive stress, respectively. It could also be shown easily that when L/Hcosθ>1, the re-entrant strut is subject to an external tensile stress, while when L/Hcosθ<1, the re-entrant strut will be subject to an external compressive stress. For the analysis of principal stress, either tensile or compressive stress can be employed for the plastic failure strength prediction as they have the same magnitude. Therefore, the first principal stress for the re-entrant struts can be determined as:

$$\sigma_1 = \frac{M_2 T}{2I_r} + \frac{F_{x2}\sin\theta - F_{z2}\cos\theta}{2A_r} + \frac{1}{2}\sqrt{\left(\frac{M_2 T}{I_r} + \frac{F_{x2}\sin\theta - F_{z2}\cos\theta}{A_r}\right)^2 + \frac{9(F_{x2}\cos\theta + F_{z2}\sin\theta)^2}{A_r^2}\left(1-\frac{4T^2}{t^2}\right)^2}$$

$$= \frac{3\tau HL^2 T\sin^2\theta}{t^4} + \frac{\tau L^2\sin\theta - \tau HL\sin\theta\cos\theta}{2t^2} + \frac{\tau L}{2t^2}\sqrt{\left(\frac{6HLT\sin^2\theta}{t^2} + L\sin\theta - H\sin\theta\cos\theta\right)^2 + 9H^2\sin^4\theta\left(1-\frac{4T^2}{t^2}\right)^2}$$

(0<T<t/2) (18)

It can be shown that the critical position of the type B re-entrant struts is located at the surface of the strut (T=t/2), and the maximum shear stress can be determined as:

$$\tau_m = \frac{\sigma_{YS}}{\frac{3HL^2\sin^2\theta}{t^3} + \frac{L^2\sin\theta}{t^2} - \frac{HL\sin\theta\cos\theta}{t^2}} \tag{19}$$

It is worth noting that the shear strength obtained from Eq.(19) only represents the lower boundary of the properties, since with many materials the structure could continue to carry more load after the initiation of yield. Fig.5 shows the relationship between the geometry designs and the shear strength of the re-entrant auxetic structure. The shear strength exhibits the same dependence on geometrical designs compared to shear modulus, which implies the possibility of achieving both high modulus and high strength with the structural designs. Also, from the analysis it appears that the vertical struts are subject to critical loading during the shearing.

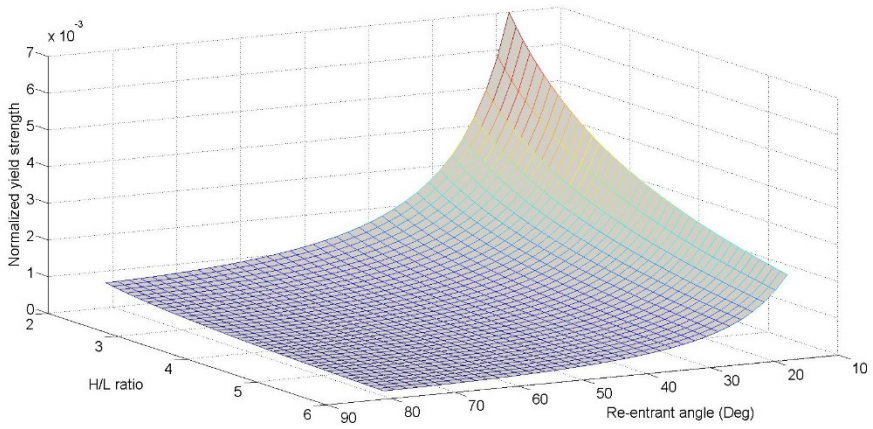

Fig.5 xz-shear strength under different geometrical designs
L=4mm, t=1mm

Shear properties in the other two principal directions

Using the same approach described in the previous sections, the shear modulus of the re-entrant auxetic structures in the other two principal directions (xy and zx directions) were also derived as functions of geometrical designs. Without showing further details, the shear modulus G_{xy} and G_{zx} were derived as:

$$G_{xy} = \frac{1}{L(H - L\cos\theta)\left(\frac{L^2}{12EI_r} + \frac{6}{5GA_r}\right)} \tag{20}$$

$$G_{zx} = \frac{1}{L\sin\theta\cos\theta(H - L\cos\theta)\left(\frac{L^2}{12EI_r} + \frac{6}{5GA_r}\right)} \tag{21}$$

With the knowledge of shear modulus, elastic modulus and Poisson's ratios in all principal directions, it becomes possible to consider the homogenization of the re-entrant auxetic structures during designs [49]. It is worth noting that the successful implementation of homogenization with the structure also depends on the boundary effects such as size effect, which will be further investigated in this study in the verification of the modeling accuracy.

Model verification

The mechanical property results from analytical modeling was first verified via finite element simulation and destructive testing. Four different design variations were created with parameters shown in Table 1. All the designed structures have struts with square cross sections, and the parameters were chosen in such a way that the effect of both relative density and auxetic behavior (Poisson's ratio) can be directly compared. For example, comparison of the effect of relative density can be made between designs A1 and A2 or B1 and B2, and the

comparison of the effect of Poisson's ratio can be made between design groups A and B, or specifically between design A2 and B2. The numbers of repetitions of unit cell is 4x4x3 (x, y, z) for A1 and A2, and 4x4x4 (x, y, z) for B1 and B2, respectively. The unit cell repetition was determined to be relatively small so the same designs can be manufactured and experimentally tested.

Design	H (mm)	L (mm)	t (mm)	θ (deg)	Rel. Dens.	PR-zx
A1	7.3	3.5	1	45	0.286	-0.937
A2	9	4.5	1	45	0.203	-0.937
B1	7	5.6	1	70	0.102	-0.302
B2	4.75	3.8	1	70	0.204	-0.302

Table 1 Design variations for model verification

The setup of the pure shear simulation is shown in Fig.6. Currently the shear simulations were only performed for xz-shearing using SolidWorks Simulation module. The designed structures were fully bonded between two rigid platens. One of the platens was fully constrained, while the other was applied a shear stress and allowed to move in the direction of the shearing. During the simulation, a shear stress of 1MPa was applied on the structure, and the maximum deformation as well as maximum stress levels were used to calculate the shear modulus and lower bound yield strength respectively. Using the default material library provided by the software, the elastic modulus, shear modulus and Poisson's ratio of Ti6Al4V-ELI were taken as 105GPa, 41GPa and 0.31 respectively.

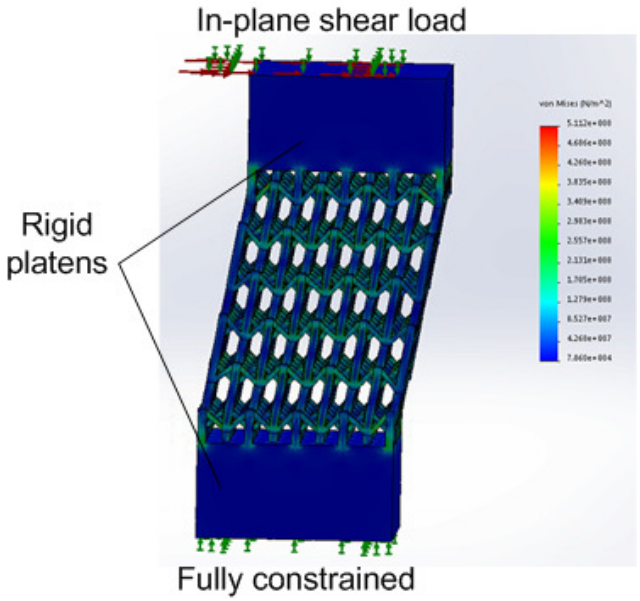

Fig.6 Setup for pure shear simulation

In order to achieve near-perfect shear testing conditions, experimental samples as shown in Fig.7 were designed, in which two cellular portions with identical designs would be subject to identical shear stress when the entire sample is subject to compressive loading. The

experimental samples were fabricated by Arcam A2 electron beam melting (EBM) system using Ti6Al4V-ELI as materials. Standard network theme was used during the fabrication, and all samples were oriented with the xz plane of the re-entrant auxetic structure normal to the build direction. The overall dimensions of the samples were measured with a caliper, and the weight of samples were also measured with a digital scale with 0.001g accuracy. In addition, the dimensions of the vertical struts and re-entrant struts were measured under optical microscope, as from earlier studies this was found to be an important source of property deviation [48, 49]. The samples were tested under an Instron universal tester. During the testing, the displacement of the crosshead was used as the sample deflection for calculation.

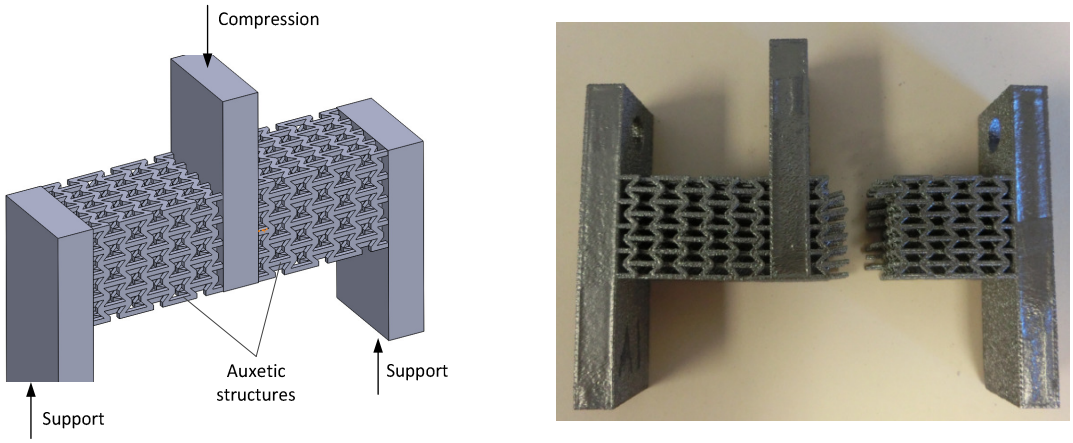

a. Sample design b. Experimental results

Fig.7 Destructive testing of samples

The dimensional measurements with the experimental samples showed good consistency. While the overall dimensions of the samples were very close to the designs, some of the strut sizes showed considerable deviations as shown in Table 2. Due to the high sensitivity of mechanical properties to the strut dimensions, both the FEA simulations and analytical model adopted the actual strut dimensions for property calculations.

Design	Vertical strut size (mm)	Re-entrant strut size (mm)
A1	0.866±0.037	0.890±0.033
A2	1.016±0.026	0.968±0.011
B1	0.992±0.024	0.983±0.176
B2	0.977±0.008	0.910±0.005

Table 2 Strut dimensions of fabricated samples

The comparison between different results are shown in Table 3. It was apparent that these exist significant difference between results from different methods. Since for both analytical model and FEA the yield strength was actually calculated within the elastic region, the results from the FEA were considered to be most accurate and used subsequently for the error analysis.

Design	Calc. Shear mod. (MPa)	Cal. Strength (MPa)	FEA shear mod. (MPa)	FEA strength (MPa)	Exp. Shear mod. (MPa)	Exp. Strength (MPa)
A1	58.3	2.5	101.4	3.2	128.0	9.4
A2	45.3	2.0	63.9	2.1	54.3	4.7
B1	40.4	0.9	23.7	0.8	15.7	1.7
B2	148	2.7	101.0	2.3	79.8	6.8

Table 3 Verification results

As was pointed out in earlier studies, there exist multiple factors that could potentially affect the modeling accuracy, including surface sintering, effective length reduction and boundary effects [47-49]. As the surface sintering was partly accounted for by using actual strut dimensions during the calculation, the investigation focused on the effective length reduction and the boundary effects. The effective length reduction is caused by the difference between a node-and-line design model (as shown in Fig.1b) and a more realistic model with strut thickness (as shown in Fig. 2b). A simulation based study was performed for the effective length reduction. As shown in Fig.8a, overhanging beams with varying tilt angles and beam lengths were designed and simulated under certain shear force F, and the struts and joints were modeled in the same way as those in the cellular structures. From the deflection results obtained from the simulations, the effective beam lengths using both Euler-Bernoulli model and Timoshenko model were calculated and compared with the designed lengths in order to obtain the effective length reduction. As shown in Fig.8b, for square beam structures with 1mm strut size, the tilt angle appears to be the only significant factor in determining the effective length reduction of the beam. As the tilt angle approaches 90°, the effective length reduction reduces to a small but non-zero value, indicating that for actual structure the joint is also contributing to the deformation of the structures.

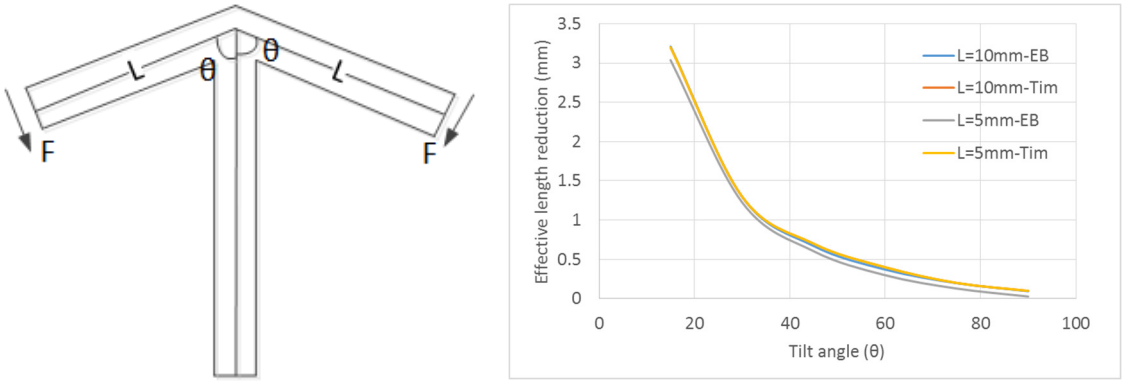

a. Simulation model b. effective length reduction

Fig.8 Effective length reduction simulation

For the various boundary effects, the size effect was investigated in this study in order to to evaluate the effect of number of unit cells on the effective mechanical properties of the structures. From previous studies it was shown that for re-entrant auxetic structures the

compressive strength and elastic modulus of the structures exhibit minimum size effect [49], which was also predicted by earlier studies with generic auxetic structures [50]. For shear modulus simulation results showed that the re-entrant auxetic structures exhibit significant size effects. As shown in Fig.9, for design A1, as the number of unit cell increases, the re-entrant auxetic structure exhibit a significant decrease of shear modulus. In addition, as the aspect ratio of the overall structure becomes large, the structure will start to behave increasingly like a long beam, which introduces additional deformation due to macroscopic bending, and the boundary condition defined in Fig.6 no longer represent a valid pure-shear condition. Therefore, the trend shown in Fig.9 might need to be subject to further scrutiny in order to obtain quantitatively accurate results.

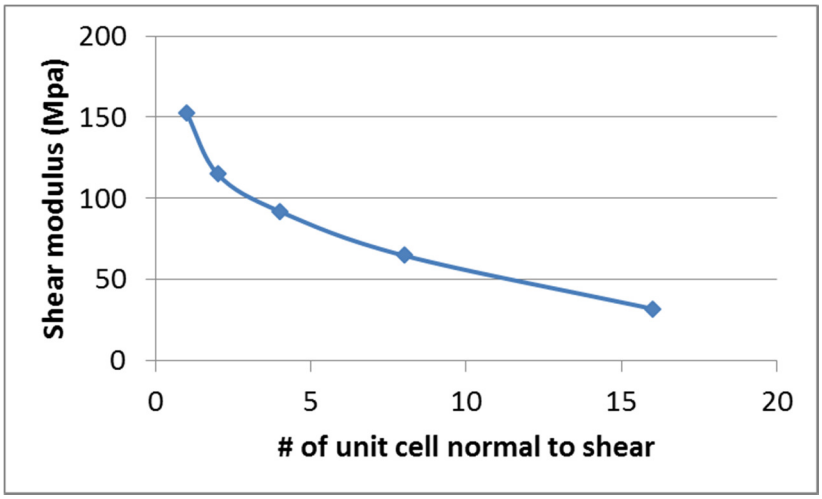

Fig.9 Size effect of shear modulus

After taking both the effective length reduction effect and the size effect into consideration, the analytical model showed significantly improved agreement with the FEA model, indicating that the analytical modeling approach is an accurate and efficient method in the design of the shear properties of the re-entrant structures. However, the results from both models still exhibit considerable deviation from the experimental results. This could potentially be contributed by several factors. First of all, the boundary constraint during the actual experimentation was not ideal. Instead of allowing for free in-plane sliding as shown in Fig.7a, the two supports were partially bonded to the bottom substrate due to the existence of friction. Secondly, the use of crosshead displacement as the measurement of sample deformation inevitably introduces error into the calculation. Thirdly, as the yield strength values from both analytical model and FEA model only indicate the lower boundary values, for ductile materials (e.g. Ti6Al4Vl used in the experimental study), the yield strength of the structures could be significantly higher.

Conclusion

In this paper the shear modulus and shear strength of the re-entrant auxetic structure were modeled based on beam bending and beam shearing. Parametric design model indicated the

feasibility of designing for structures that possess both high shear modulus and high shear strength, which could be valuable for potential sandwich applications. The analytical model also yields satisfactory accuracy when size effect and effective length reduction effect are taken into consideration properly. On the other hand, it was observed that the re-entrant auxetic structure exhibit significant size effect upon shearing, which is very different with its compressive/tensile properties. This size effect also indicates that the homogenization of this structure could not be readily achieved based on the analytical modeling approach. As the homogenization ability of a cellular structure is an intrinsic characteristic, it could be expected that during the design of this re-entrant auxetic structures, more sophisticated design approach might be necessary, and further works are needed to address this.

Acknowledgement

The authors are grateful of the support from Rapid Prototyping Center (RPC) at University of Louisville, and shear experiments by Shanshan Zhang.

Reference

[1] T. M. McCormack, R.Miller, O. Kesler, L. J. Gibson. Failure of sandwich beams with metallic foam cores. International Journal of Solids and Structures. 38(2001): 4901-4920.

[2] Lorna J. Gibson. Cellular solids: structure and properties, 2nd edition. Cambridge University Press, New York, NJ, USA. 1997.

[3] M. F. Ashby, A. G. Evans, N. A. Fleck, L. J. Gibson, J. W. Hutchinson, H. N. G. Wadley. Metal Foams: A Design Guide. Butterworth-Heinemann, Woburn, MA, USA. 2000.

[4] E. Andrews, W. Sanders, L. J. Gibson. Compressive and tensile behaviour of aluminum foams. Materials Science and Engineering A. 270(1999): 113-124.

[5] V. Crupi, R. Montanini. Aluminum foam sandwiches collapse modes under static and dynamic three-point bending. International Journal of Impact Engineering. 34(2007): 509-521.

[6] H. G. Allen. Analysis and design of structural sandwich panels. Pergamon Press, Oxford, UK. 1969.

[7] C. Chen, A-M Harte, N. A. Fleck. The plastic collapse of sandwich beams with a metallic foam core. International Journal of Mechanical Sciences. 43(2001): 1483-1506.

[8] M. Grediac. A finite element study of the transverse shear in honeycomb cores. International Journal of Solids and Structures. 30(1993): 1777-1788.

[9] Joseph F. Rakow, Anthony M. Waas. Size effects and the shear response of aluminum foam. Mechanics of Materials. 37(2005): 69-82.

[10] O. Kesler, L. J. Gibson. Size effects in metallic foam core sandwich beams. Materials Science and Engineering A. 326(2002): 228-234.

[11] C. Tekoglu, P. R. Onck. Size effects in the mechanical behavior of cellular materials. Journal of Materials Science. 40(2005): 5911-5917.

[12] P. R. Onck, E. W. Andrews, L. J. Gibson. Size effects in ductile cellular solids. Part I: modeling. International Journal of Mechanical Sciences. 43(2001): 681-699.

[13] E. W. Andrews, G. Gioux, P. Onck, L. J. Gibson. Size effects in ductile cellular solids. Part II: experimental results. International Journal of Mechanical Sciences. 43(2001): 701-713.

[14] F. E. Sezgin, M. Tanoglu, O. O. Egilmez, C. Donmez. Mechanical Behavior of Polypropylene-based Honeycomb-Core Composite Sandwich Structures. Journal of Reinforced Plastics and Composites. 29(2010): 1569-1579.

[15] L. J. Gibson, M. F. Ashby, J. Zhang, T. C. Triantafillou. Failure surfaces for cellular materials under multiaxial loads – I. Modelling. International Journal of Mechanical Sciences. 31(1989): 635-663.

[16] W. E. Warren, A. M. Kraynik. Foam mechanics: the linear elastic response of two-dimensional spatially periodic cellular materials. Mechanics of Materials. 6(1987): 27-37.

[17] A. –J. Wang, R. S. Kumar, D. L. McDowell. Mechanical Behavior of Extruded Prismatic Cellular Metals. Mechanics of Advanced Materials and Structures. 12(2005): 185-200.

[18] Chae-Hong Lim, Insu Jeon, Ki-Ju Kang. A new type of sandwich panel with periodic cellular metal cores and its mechanical performances. Materials and Design. 30(2009): 3082-3093.

[19] H. L. Fan, F. N. Jin, D. N. Fang. Nonlinear mechanical properties of lattice truss materials. Materials and Design. 30(2009): 511-517.

[20] Gregory W. Kooistra, Douglas T. Queheillalt, Haydn N. G. Wadley. Shear behavior of aluminum lattice truss sandwich panel structures. Mechanical Science and Engineering A. 472(2008): 242-250.

[21] Hailong Chen, Qing Zheng, Long Zhao, Yu Zhang, Hualin Fan. Mechanical Property of lattice truss material in sandwich panel including strut flexural deformation. Composite Structure. 2012. In press.

[22] Yuki Sugimura. Mechanical response of single-layer tetrahedral trusses under shear loading. Mechanics of Materials. 36(2004): 715-721.

[23] J. C. Wallah, L. J. Gibson. Defect sensitivity of a 3D truss material. Scripta Materialia. 45(2001): 639-644.

[24] V. S. Dashpande, N. A. Fleck. Collapse of truss core sandwich beams in 3-point bending. International Journal of Solids and Structures. 38(2001): 6275-6305.

[25] V. S. Dashpande, N. A. Fleck, M. F. Ashby. Effective properties of the octet-truss lattice material. Journal of the Mechanics and Physics of Solids. 49(2001): 1747-1769.

[26] T. Liu, Z. C. Deng, T. J. Lu. Design optimization of truss-cored sandwiches with homogenization. International Journal of Solids and Structures. 43(2006): 7891-7918.

[27] H. J. Rathburn, F. W. Zok, A. G. Evans. Strength optimization of metallic sandwich panels subject to bending. International Journal of Solids and Structures. 42(2005): 6643-6661.

[28] Roderic Lakes. Foam Structures with a Negative Poisson's Ratio. Science. 235(1987): 1038-1040.

[29] F. Scarpa, P. J. Tomlin. On the transverse shear modulus of negative Poisson's ratio lattice structures. Fatigue & Fracture of Engineering Materials & Structures. 23(2000): 717-720.

[30] F. Scarpa, G. Tomlinson. Theoretical characteristics of the vibration of sandwich plates with in-plane negative Poisson's ratio values. Journal of Sound and Vibration. 230(2000): 45-67.

[31] R. S. Lakes, K. Elms. Indentability of Conventional and Negative Poisson's Ratio Foams. Journal of Composite Materials. 27(1993): 1193-1202.

[32] K. L. Alderson, V. R. Simkins, V. L. Coenen, et al. How to make auxetic fibre reinforced composites. Physica Status Solidi (b). 57(2009): 1865-1874.

[33] R. S. Lakes. Design Considerations for Materials with Negative Poisson's Ratios. Journal of Mechanical Design. 115(1993): 676-700.

[34] Abderrezak Bezazi, Fabrizio Scarpa. Tensile fatigue of conventional and negative Poisson's ratio open cell PU foams. International Journal of Fatigue. 31(2009): 488-494.

[35] Abderrezak Bezazi, Fabrizio Scarpa. Mechanical behaviour of conventional and negative Poisson's ratio thermoplastic polyurethane foams under compressive cyclic loading. International Journal of Fatigue. 29(2007): 922-930.

[36] F. Scarpa, P. Pastorino, A. Garelli, et al. Auxetic compliant flexible PU foams: static and dynamic properties. Physica Status Solidi (b). 242(2005): 681-684.

[37] F. Scarpa, L. G. Ciffo, J. R. Yates. Dynamic properties of high structural integrity auxetic open cell foam. Smart Materials and Structures. 13(2004): 49-56.

[38] Alessandro Spadoni, Massimo Ruzzene. Numerical and experimental analysis of the static compliance of chiral truss-core airfoils. Journal of Mechanics of Materials and Structures. 2(2007): 965-981.

[39] A. Spadoni, M. Ruzzene. Static Aeroelastic Response of Chiral-core Airfoils. Journal of Intelligent Material Systems and Structures. 18(2007): 1067-1075.

[40] D. Bornengo, F. Scarpa, C. Remillat. Evaluation of hexagonal chrial structure for morphing airfoil concept. Proceedings of the Institution of Mechanical Engineers, Part G: Journal of Aerospace Engineering. 219(2005): 185-192.

[41] Hyeonu Heo, Jaehyung Ju, Doo-Man Kim, Chang-Soo Jeon. Passive morphing airfoil with honeycombs. Proceedings of the ASME 2011 International Engineering Congress & Exhibition, IMECE 2011. Denver, CO, USA.

[42] Paolo Bettini, Alessandro Airoldi, Giuseppe Sala, Luca Di Landro, Massimo Ruzzene, Alessandro Spadoni. Composite chiral structures for morphing airfoils: Numerical analysis and development of a manufacturing process. Composites: Part B. 41(2010): 133-147.

[43] F. Scarpa, P. J. Tomlin. On the transverse shear modulus of negative Poisson's ratio honeycomb structures. Fatigue and Fracture of Engineering Materials and Structures. 23(2000): 717-720.

[44] C. Lira, F. Scarpa. Transverse shear stiffness of thickness gradient honeycombs. Composite Science and Technology. 70(2010): 930-936.

[45] C. Lira, P. Innocenti, F. Scarpa. Transverse elastic shear of auxetic multi re-entrant honeycombs. Composite Structures. 90(2009): 314-322.

[46] X. Frank Xu, Pizhong Qiao, Julio F. Davalos. Transverse shear stiffness of composite honeycomb core with general configuration. Journal of Engineering Mechanics. 127(2001): 1144-1151.

[47] Li Yang, Ola Harrysson, Harvey West, Denis Cormier. Compressive properties of Ti-6Al-4V auxetic mesh structures made by electron beam melting. Acta Materialia. 60(2012): 3370-3379.

[48] Li Yang, Ola Harrysson, Harvey West, Denis Cormier. Modeling of uniaxial compression in a 3D periodic re-entrant lattice structure. Journal of Materials Science. 48(2013): 1413-1422.

[49] Li Yang, Ola Harrysson, Harvey West, Denis Cormier. Mechanical properties of 3D re-entrant honeycomb auxetic structures realized via additive manufacturing. International Journal of Solids and Structures. 69-70(2015): 475-490.

[50] R. S. Lakes. Design considerations for materials with negative Poisson's ratios. Transactions of ASME: Journal of Mechanical Design. 115(1993): 696-700.